Angewandte Chemie
Eine Zeitschrift der Gesellschaft Deutscher Chemiker

Supporting Information

69451 Weinheim, Germany

Concerted Proton-Electron Transfer in Pyridyl-Phenols: The Importance of the Hydrogen Bond

Todd F. Markle and James M. Mayer*

University of Washington, Department of Chemistry,
Box 351700, Seattle, WA 98195, mayer@chem.washington.edu

Table of Contents:

I. General Experimental

Unless otherwise noted, reagents were purchased from Aldrich, solvents from Fischer, and deuterated solvents from Cambridge. MeCN was purchased from Burdick and Jackson (low-water brand) and stored in an argon-pressurized stainless steel drum plumbed directly into a glovebox. Tetrabutylammonium hexafluorophosphate was recrystallized three times from EtOH and dried *in vacuo* for two days at 110 °C prior to use. Isopropylmagnesium chloride (2.0 M in THF) was purchased from Acros. The iron-bipyridyl and phenanthroline complexes were synthesized according to literature procedures[1] and were used as PF_6^- salts. Triarylaminium salts were prepared from the corresponding amines as described previously.[2]

^{1}H NMR and ^{13}C NMR spectra were recorded on Bruker AV300, AV301, DRX499 or AV500 spectrometers at ambient temperatures; chemical shifts are reported relative to TMS in ppm by referencing to the residual solvent signals. Column chromatography used silica gel as the stationary phase. Infrared spectra were obtained on a Bruker Vector 33 or a Perkin Elmer 1720 spectrometer. Mass spectrometry was performed on a Bruker Esquire Ion Trap Mass Spectrometer using electrospray ionization.

II. Synthesis of HOAr-CH_2py.

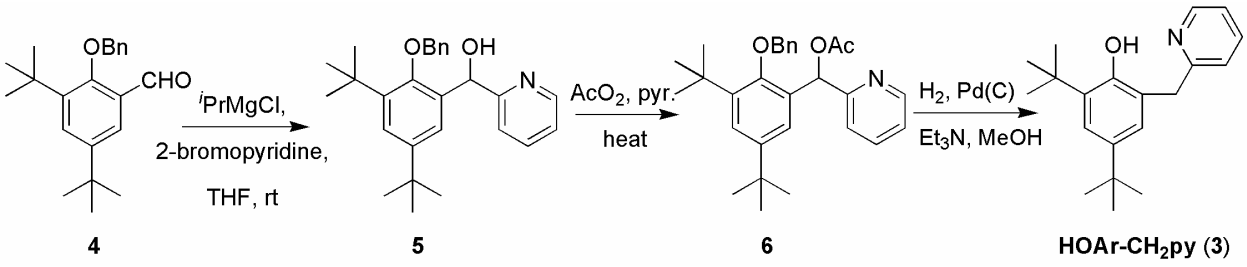

Compound **4** was prepared from commercially available 3,5-di-*tert*-butyl-2-hydroxybenzaldehyde as previously described.[3]

(2-Benzyloxy-3,5-di-*tert*-butyl-phenyl)-pyridin-2-yl-methanol (5). Following literature precedent, isopropyl magnesium chloride (3.15 mL of 2.0 M THF solution, 6.3 mmol) was added dropwise to a round bottom flask containing a solution of 2-bromopyridine (0.60 mL, 6.3 mmol) in 10 mL anhydrous THF and the mixture was stirred at room temperature under N_2.[4] After 2 h, **4** (2.04 g, 6.3 mmol) was added as a solution in dry THF (10 mL) and the reaction mixture was stirred at room temperature under N_2. After 16 h, the reaction was quenched with water (10 mL) and diethyl ether was added to yield a biphasic mixture. The aqueous layer was washed with Et_2O (3 × 20 mL). The combined organic extracts were washed with 10% $HCl_{(aq)}$ followed by brine and dried over $MgSO_4$ then the solvent was removed under vacuum. Column chromatography (10% EtOAc/hexanes) gave **5** (0.51 g, 50% yield) as a pale yellow oil. ^{1}H NMR

(1) DeSimone, R. E.; Drago, R. S. *J. Am. Chem. Soc.* **1970,** *92,* 2343-2352.
(2) Rhile, I. J.; Markle, T. F.; Nagao, H.; DiPasquale, A. G.; Lam, O. P.; Lockwood, M. A.; Rotter, K.; Mayer, J. M. *J. Am. Chem. Soc.* **2006**, *128*, 6075-6088, and references therein.
(3) Ryu, H.-K.; Kim, W.-Y.; Nahm, K. S.; Hahn, Y. B.; Lee, Y. S.; Lee, C. *Synthetic Metals.* **2002**, *128*, 21-25.
(4) Trécourt**,** F.; Breton, G.; Bonnet, V.; Mongin, F.; Marsais, F.; Quèguiner, G. *Tetrahedron*. **2000,** *56*, 1349-1360**.**

δ: 8.54 (d, 1H, *J* = 5.0), 7.61 – 7.53 (m, 3H), 7.42 – 7.33(m, 4H), 7.18 (m, 1H), 7.09 (d, *J* = 7.9 Hz, 1H), 7.01 (d, *J* = 2.3 Hz, 1H), 6.22 (s, 1H, C*H*), 5.59 (s, br, 1H), 5.32 (d, *J* = 12.1 Hz, 1H), 5.13 (d, *J* = 12.1 Hz, 1H), 1.48 (s, 9 H), 1.21 (s, 9 H). $^{13}C\{^{1}H\}$ NMR ($CDCl_3$): δ 161.6, 154.4, 147.2, 146.6, 142.3, 138.2, 137.1, 136.4, 128.7, 127.8, 127.1, 124.45, 124.44, 122.4, 122.1 (aryl carbons); 77.4 (*C*H); 69.0 (*C*H_2); 35.8, 34.8 (*C*Me_3); 31.6 (^{t}Bu *C*H_3's) [the two ^{t}Bu methyl resonances are overlapping]. MS (ESI, *m/z*) 404 (M+H), 386 (M-OH).

Acetic acid (2-benzyloxy-3,5-di-*tert*-butyl-phenyl)-pyridin-2-yl-methyl ester (**6**). The benzyl alcohol **5** (1.0 g, 2.5 mmol) was dissolved in 5 mL of pyridine and acetic anhydride (1:1) and heated to 100 °C under N_2 for 20 min. The volatiles were removed under vacuum yielding an amber oil which solidified on the benchtop to give a beige solid which was used without further purification. An analytical sample was purified on a silica column using 9:1 hexanes/EtOAc. ^{1}H-NMR ($CDCl_3$) δ: 8.58 (m, 1 H), 7.62 – 7.58 (m, 3H), 7.42 – 7.12 (m, 8H), 5.18(d, *J* = 11.8 Hz, 1H), 5.11 (d, *J* = 11.8 Hz, 1H), 2.20 (s, 3H), 1.44 (s, 9H), 1.28 (s, 9H). $^{13}C\{^{1}H\}$ NMR ($CDCl_3$): δ 170.4 [O*C*(O)Me], 159.3, 154.0, 149.3, 146.5, 142.6, 137.9, 139.9, 132.3, 128.7, 127.9, 127.5, 125.4, 124.8, 122.6, 121.8 (aryl carbons); 76.9 (*C*H); 72.8 (*C*H_2); 35.8, 34.9 (*C*Me_3); 31.7 (^{t}Bu *C*H_3's); 21.5 [OC(O)*C*H_3] [the two ^{t}Bu methyl resonances are overlapping]. MS (ESI, *m/z*) 446 (M+H), 386 (M-CH_3CO_2).

2,4-Di-*tert*-butyl-6-pyridin-2-ylmethyl-phenol (**HOAr-CH_2py**). A solution of **6** (1.1 g, 2.5 mmol) in EtOH (30 mL) containing Et_3N (0.73 mL, 5.0 mmol) was agitated on a Parr apparatus under H_2 (50 psi) in the presence of Pd(C) (10 mol%). After 50 h the reaction mixture was filtered through Celite and the volatiles were removed on the rotovap. Column chromatography (5% EtOAc in hexanes) yielded **HOAr-CH_2py** (0.67 g, 2.3 mmol, 92% yield) as a white solid. X-ray quality crystals were obtained by slow evaporation of a hexane solution. ^{1}H NMR (CD_3CN): δ 11.15 (s, 1 H, O*H*), 8.45 (m, 1 H, 6'-H), 7.80-7.75 (m, 1 H, 6'-*H*), 7.44 (d, *J* = 7.8 Hz, 1H, 3'-*H*), 7.25 (m, 1H, 5'-*H*), 7.18 (d, *J* = 2.6 Hz, 1H, Ar-*H*), 7.14 (d, *J* = 2.6 Hz, 1H, Ar-*H*), 4.06 (s, 2H, CH_2), 1.41 (s, 9H, C(CH_3)$_3$), 1.26 (s, 9H, C(CH_3)$_3$). $^{13}C\{^{1}H\}$ NMR (CD_3CN): δ 163.0, 154.0, 149.1, 143.0, 140.1, 138.9, 128.4, 126.4, 124.1, 123.9, 123.5 (aryl carbons); 42.3 (*C*H_2); 36.1, 35.2, (*C*Me_3); 32.3, 30.5 (^{t}Bu *C*H_3's). MS (ESI, *m/z*) 298 (M+H).

III. V. X-ray Crystal Structures of HOAr-CH_2py.

General procedure. A colorless block 0.15 x 0.10 x 0.10 mm in size was mounted on a Cryoloop with Paratone oil. Data were collected in a nitrogen gas stream at 100(2) K using omega scans. Crystal-to-detector distance was 60 mm and exposure time was 20 seconds per frame using a scan width of 0.3°. Data collection was 100.0% complete to 25.00° in θ. A total of 14832 reflections were collected covering the indices, $-13 \leq h \leq 12$, $-21 \leq k \leq 22$, $-14 \leq l \leq 14$. 4078 reflections were found to be symmetry independent, with an R_{int} of 0.0236. Indexing and unit cell refinement indicated a primitive, monoclinic lattice. The space group was found to be $P2_1/n$ (No. 14). The data were integrated using the Bruker SAINT software program and scaled using the SADABS software program. Solution by direct methods (SIR-2004) produced a complete heavy-atom phasing model consistent with the proposed structure. All non-hydrogen atoms were refined anisotropically by full-matrix least-squares (SHELXL-97). All hydrogen atoms, with the exception of the hydroxyl hydrogen H1, were placed using a riding model. Their positions were constrained relative to their parent atom using the appropriate HFIX command in SHELXL-97. The hydroxyl hydrogen H1 was located from the difference map and its location refined isotropically. Collection and refinement data are given in Table S1. Data for the hydrogen bonds in the molecules are listed in Table S2. An ORTEP is shown in Figure S1.

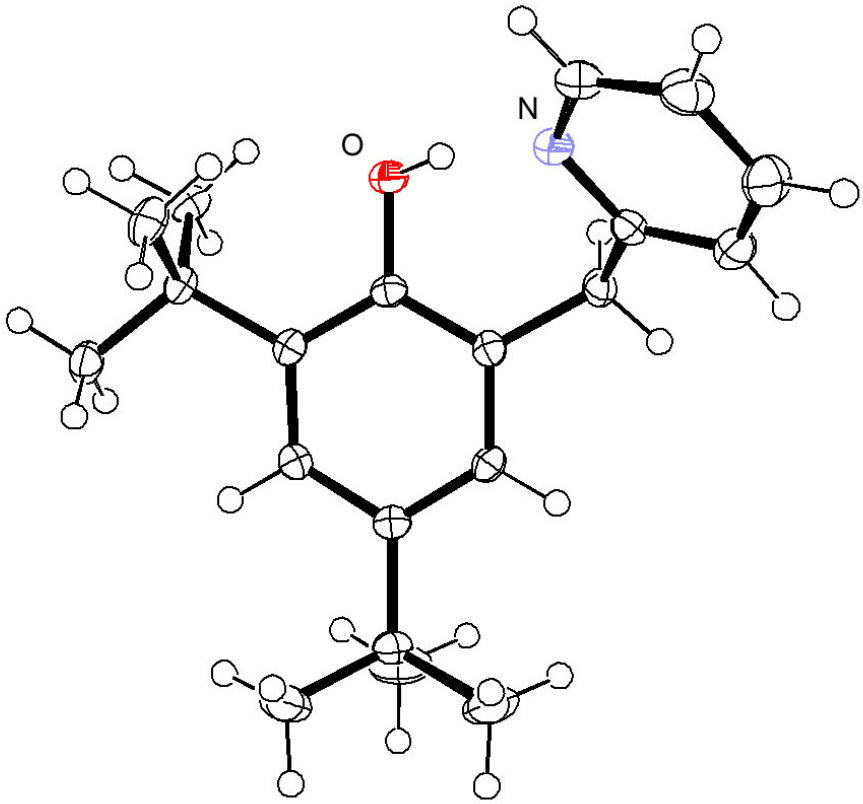

Figure S1. ORTEP depicting the crystallographic structure of **HOAr-CH_2py**.

Table S1. Collection and refinement data.

Empirical formula	C20 H27 N O	
Formula weight	297.43	
Temperature (K)	100(2)	
Wavelength (Å)	0.71073	
Crystal system	Monoclinic	
Space group	$P2_1/n$	
Unit cell dimensions (Å,˚)	a = 10.1110(7)	α = 90
	b = 16.7180(12)	β = 109.3150(10)
	c = 11.0080(8)	γ = 90
Volume	1756.0(2) Å^3	
Z	4	
Density (calculated)	1.125 Mg/m^3	
Absorption coefficient	0.068 mm^{-1}	
F(000)	648	
Crystal size (mm)	0.15 × 0.10 × 0.10	
Crystal color/habit	colorless block	
Theta range for data collection (˚)	2.31 to 28.21	
Index ranges	$-13 \le h \le 12$, $-21 \le k \le 22$, $-14 \le l \le 14$	
Reflections collected	14832	
Independent reflections	4078 [R_{int} = 0.0236]	
Completeness to theta = 25.00°	100.0 %	
Absorption correction	Semi-empirical from equivalents	
Max. and min. transmission	0.9932 and 0.9899	
Refinement method	Full-matrix least-squares on F^2	
Data / restraints / parameters	4078 / 0 / 208	
Goodness-of-fit on F^2	1.021	
Final R indices [I > 2σ(I)]	R_1 = 0.0463, wR_2 = 0.1237	
R indices (all data)	R_1 = 0.0526, wR_2 = 0.1289	
Largest diff. peak and hole (e Å^{-3})	0.428 and -0.187	

Table S2. Hydrogen bonding parameters for HOAr-CH$_2$py (distances in Å, angles in ˚).

d(O-H)	*d*(H•••N)	*d*(O•••N)	∠(OHN)
0.923(17)	1.782(17)	2.6914(13)	167.7(15)

IV. Infrared spectroscopy

Vibrational spectra (Figures 1, S2-S4) were collected as solutions (0.18 M) in dry acetonitrile or CCl_4 in a cell with NaCl or ZnSe windows and as a KBr pellet. The identity of the phenolic OH stretching band was confirmed by analysis of the deutero analogues, **DOAr-B,** which were prepared by adding d_4-methanol to a solution of **HOAr-B** in dry Et_2O followed by removal of solvents *in vacuo*. This process was repeated a total of three times. In the case of **HOAr-CH$_2$py**, KBr spectra obtained from crystals grown in a similar manner to that which yielded the X-ray structure were indistinguishable from spectra obtained from powder. Broad, structured OH stretching bands are common in hydrogen bonded systems.[5]

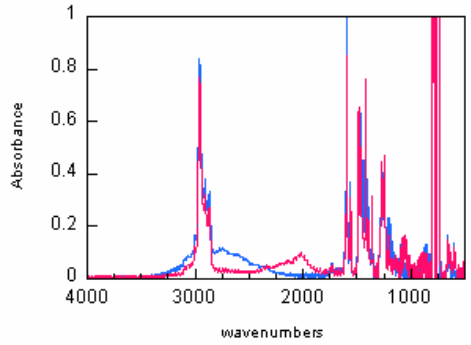

Figure S2. IR spectra of **HOAr-py** (blue) and **DOAr-py** (red) in CCl_4.

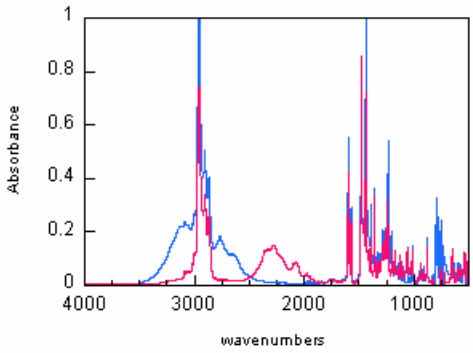

Figure S3. IR spectra of **HOAr-CH$_2$py** (blue) and **DOAr-CH$_2$py** (red) in CCl_4.

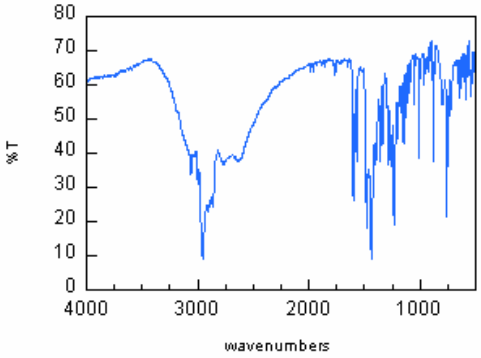

Figure S4. IR spectrum of crystalline **HOAr-CH$_2$py** as a KBr pellet.

(5) Bratos, S; Leicknam, J-Cl; Gallot, G; Ratajczak, H, in *Ultafast Hydrogen Bonding Dynamics and Proton Transfer Processes in the Condensed Phase*, eds Elsaaesser, T; Bakker, H J. Kluwer Academic, Boston, **2002**, pp 5-30.

V. Electrochemistry

Cyclic voltammograms (Figure S5) were taken on an E2 Epsilon electrochemical analyzer (Bioanalytical Systems) at ca. 5 mM substrate in anaerobic 0.1 M $^{n}Bu_4NPF_6$ acetonitrile solution. The electrodes were as follows: working, glassy carbon; auxiliary, platinum wire; and reference, $Ag/AgNO_3$ (0.01 M) in electrolyte solution. All potentials are reported vs. a $Cp_2Fe^{+/0}$ internal standard. Errors are estimated to be ±0.02V.

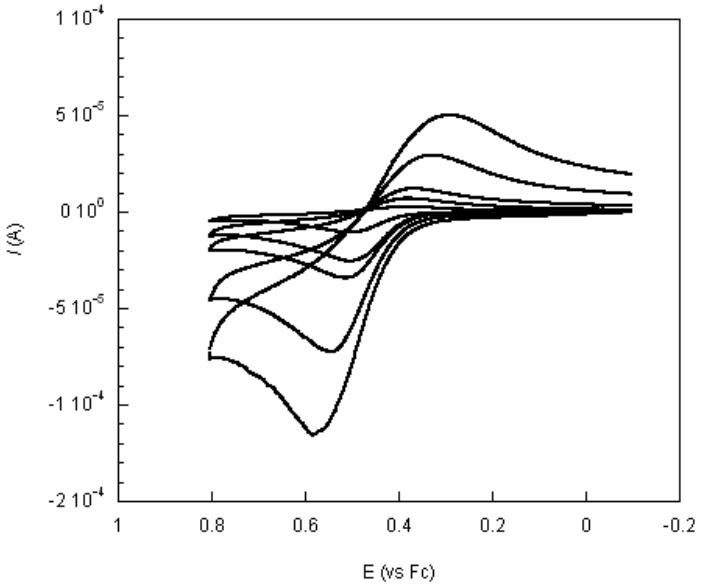

Figure S5. Cyclic voltammograms of **HOAr-CH_2py** at ν = 12, 25, 50, 100, 200, and 500 mV s^{-1}.

VI. Kinetics.

Kinetics experiments were performed on an OLIS RSM-1000 stopped-flow in anaerobic MeCN. The data were analyzed with SpecFit™ global analysis software.[6] Kinetics were fit to pseudo-first order, second order, or opposing second order kinetics as appropriate. Kinetics for the reactions utilizing iron(III) oxidants were obtained at 0.1 M $^{n}Bu_4NPF_6$ as the potentials for these compounds vary with ionic strength due to ion pairing.[7]

A. **HOAr-CH$_2$py** + $[Fe(N\text{-}N)_3]^{3+}$, and $[NAr_3]^{\bullet+}$ at room temperature.

The kinetics for reaction of **HOAr-CH$_2$py** + $[Fe(3,4,7,8\text{-}Me_4phen)_3](PF_6)_3$ were performed under pseudo-first order conditions with 8-40-fold excess of phenol, and fit to first-order kinetics. The observed rate constants at individual concentrations are reported on Table S3 and plotted in Figure S6. The slope of k_{obs} v. [**HOAr-CH$_2$py**] is reported as the second-order rate constant.

Table S3. Second-order rate constants for **HOAr-CH$_2$py** + $[Fe(3,4,7,8\text{-}Me_4phen)_3]^{3+}$.

[**HOAr-CH$_2$py**][a]	k_{obs} (s^{-1})	σ
0.20	4.2	0.03
0.41	8.3	0.07
0.61	13.5	0.17
0.82	18.4	0.37
1.0	25.5	1.09

[a] mM.

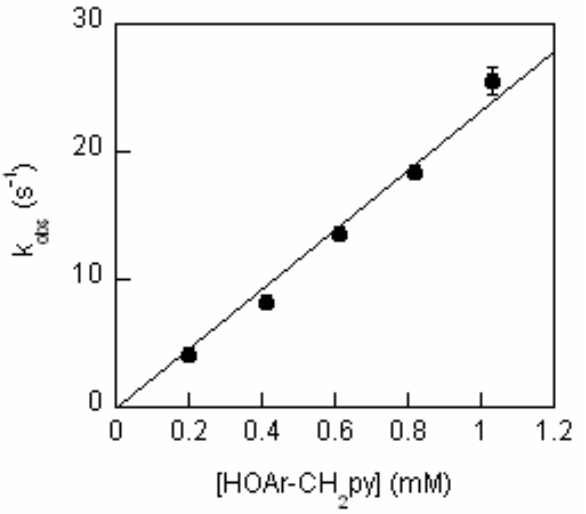

Figure S6. Pseudo first-order rate constants vs. concentration of phenol for **HOAr-CH$_2$py** + $[Fe(3,4,7,8\text{-}Me_4phen)_3]^{3+}$.

(6) Binstead, R. A.; Zuberbühler, A.D.; Jung, B. *Specfit™,* version 3.0.36 (32-bit Windows); Spectrum Software Associates: Chapel Hill, NC, 2004.

(7) (a) Noel, M.; Vasu, K. I. *Cyclic Voltammetry and the Frontiers of Electrochemistry*; Aspect: London, 1990; pp. 141-143. (b) Braga, T. G.; Wahl, A. C. *J. Phys. Chem.* **1985,** *89,* 5822-5828. (c) Chan, M.-S.; Wahl, A. C. *J. Phys. Chem*. **1978,** *82,* 2542-2549.

The kinetics for reaction of **HOAr-CH$_2$py** + [Fe(4,7-Me$_2$phen)$_3$](PF$_6$)$_3$ were performed under pseudo-first order conditions with 5-30-fold excess of phenol, and fit to first-order kinetics. The observed rate constants at individual concentrations are reported on Tables S4 and plotted in Figure S7. The slope of k_{obs} v. [**HOAr-CH$_2$py**] is reported as the second-order rate constant.

Table S4. Second-order rate constants for **HOAr-CH$_2$py** + [Fe(4,7-Me$_2$phen)$_3$]$^{3+}$.

[**HOAr-CH$_2$py**][a]	k_{obs} (s^{-1})	σ
0.27	73	3.1
0.55	139	5.1
0.82	219	6.1
1.09	270	6.2
1.37	350	26.7

[a] mM.

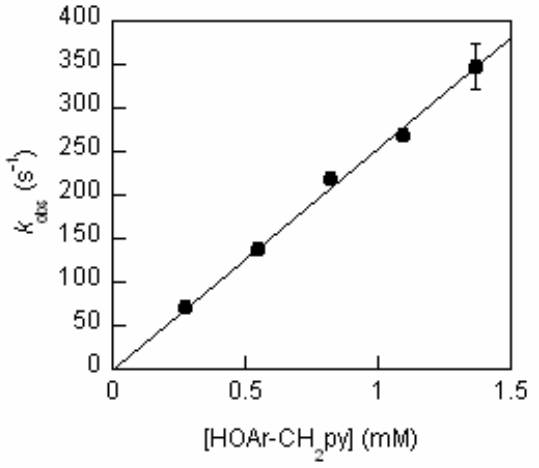

Figure S7. Pseudo first-order rate constants vs. concentration of phenol for **HOAr-CH$_2$py** + [Fe(4,7-Me$_2$phen)$_3$]$^{3+}$.

The kinetics for reaction of **HOAr-CH$_2$py** + [Fe(5,5'-Me$_2$bpy)$_3$](PF$_6$)$_3$ were performed under pseudo-first order conditions with 10-50-fold excess of phenol, and fit to first-order kinetics. The observed rate constants at individual concentrations are reported on Table S5 and plotted in Figure S8. The slope of k_{obs} v. [**HOAr-CH$_2$py**] is reported as the second-order rate constant.

Table S5. Second-order rate constants for **HOAr-CH$_2$py** + [Fe(5,5'-Me$_2$bpy)$_3$]$^{3+}$.

[**HOAr-CH$_2$py**][a]	k_{obs} (s^{-1})	σ
0.27	42	3.4
0.55	78	5.5
0.82	133	0.9
1.1	180	12
1.4	240	30

[a] mM.

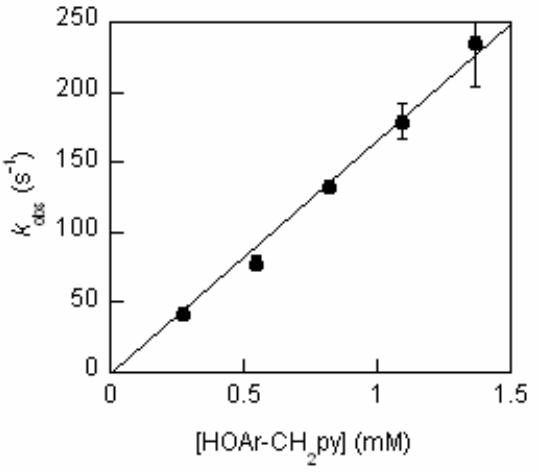

Figure S8. Pseudo first-order rate constants vs. concentration of phenol for **HOAr-CH$_2$py** + [Fe(5,5'-Me$_2$bpy)$_3$]$^{3+}$.

The rate constants for reaction of **HOAr-CH$_2$py** with [Fe(bpy)$_3$](PF$_6$)$_3$, and N(*p*-C$_6$H$_4$OMe)(*p*-C$_6$H$_4$Br)$_2$PF$_6$ were measured with 2-10-fold excess of phenol, and fit to opposing second-order kinetics. The rate constants for the two reactions at individual concentrations are reported in Tables S6 and S7 and plotted in Figures S9 and S10.

Table S6. Second-order rate constants for **HOAr-CH$_2$py** + [Fe(bpy)$_3$](PF$_6$)$_3$.

[phenol][a]	k (M^{-1} s^{-1})	σ
0.031	2.83×10^6	6.0×10^4
0.062	2.13×10^6	5.5×10^4
0.093	2.10×10^6	8.0×10^4
0.16	1.93×10^6	6.2×10^4

[a] (mM)

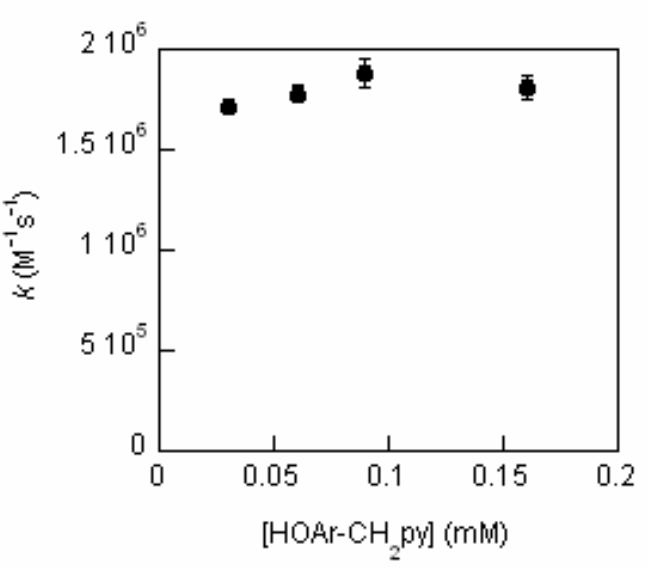

Figure S9. Second-order rate constants vs. concentration of phenol for [Fe(bpy)$_3$](PF$_6$)$_3$.

Table S7. Second-order rate constants for **HOAr-CH$_2$py** + N(*p*-C$_6$H$_4$OMe)(*p*-C$_6$H$_4$Br)$_2$PF$_6$.

[phenol][a]	k (M^{-1} s^{-1})	σ
0.031	5.08×10^5	1900
0.062	5.37×10^5	2300
0.093	5.41×10^5	9100
0.12	5.33×10^5	8300
0.16	5.31×10^5	12000

[a] (mM)

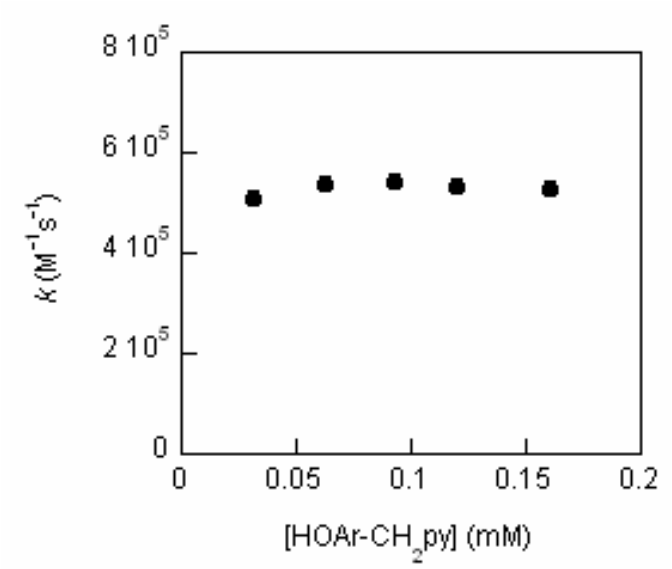

Figure S10. Second-order rate constants vs. concentration of phenol for N(*p*-C$_6$H$_4$OMe)(*p*-C$_6$H$_4$Br)$_2$PF$_6$.

The rate constants for reaction of **HOAr-CH$_2$py** with N(*p*-$C_6H_4OMe)_3PF_6$, and N(*p*-$C_6H_4Me)_3PF_6$ were measured with 10-50-fold excess of phenol, and fit to opposing second-order kinetics. The rate constants for the two reactions at individual concentrations are reported in Table S8 and S9 and plotted in Figures S11 and S12.

Table S8. Second-order rate constants for **HOAr-CH$_2$py** + N(*p*-$C_6H_4OMe)_3PF_6$.

[phenol][a]	k (M^{-1} s^{-1})	σ
0.21	810	18
0.41	780	14
0.62	750	25
0.83	770	14
1.04	752	6

[a] (mM)

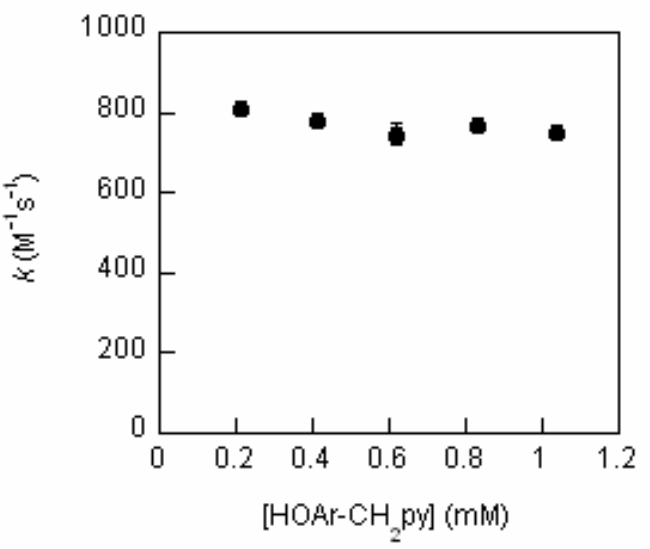

Figure S11. Second-order rate constants vs. concentration of phenol for N(*p*-$C_6H_4OMe)_3PF_6$.

Table S9. Second-order rate constants for **HOAr-CH$_2$py** + N(*p*-$C_6H_4Me)_3PF_6$.

[phenol][a]	k (M^{-1} s^{-1})	σ
0.27	1.13×10^5	6.5×10^3
0.55	1.24×10^5	1.1×10^3
0.82	1.29×10^5	7.6×10^3
1.1	1.27×10^5	3.7×10^3
1.4	1.15×10^5	1.0×10^4

[a] (mM)

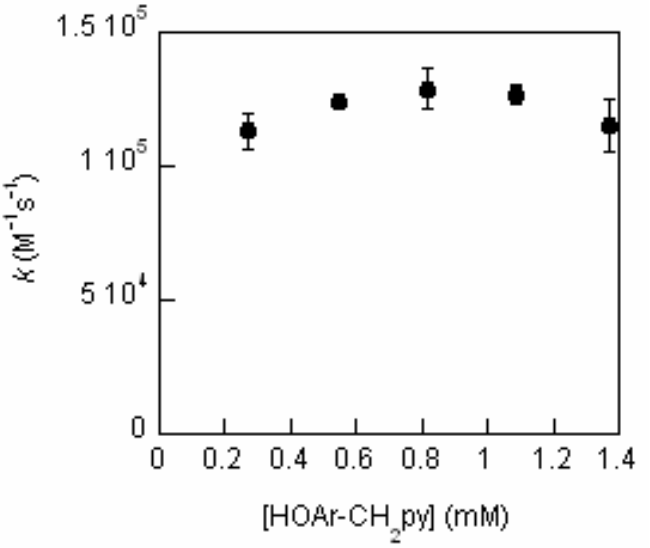

Figure S12. Second-order rate constants vs. concentration of phenol for N(*p*-$C_6H_4Me)_3PF_6$.

Bi-molecular rate constants (k) are plotted vs. E_{rxn} (Table 1) for the r.t. reactions of **HOAr-CH$_2$py** with $[NAr_3]^{+\bullet}$ are plotted in Figure S13. Here, Ar_3 = (p-$C_6H_4OMe)_3$, (p-$C_6H_4Me)_3$, and (p-C_6H_4OMe)(p-$C_6H_4Br)_2$. The line to guide the eye is equation 1 with log Z = 9.5 and λ = 21.6 kcal mol^{-1}. Log k vs. E_{rxn} data for the reactions of **HOAr-C(Ph)$_2$NH$_2$** + $[NAr_3]^{+\bullet}$ (from reference 2) are included in Figure S13 for comparison. Rate constants for reactions of **HOAr-py** + $[NAr_3]^{+\bullet}$ have not been determined, they are apparently too fast to be measured with our stopped-flow apparatus.[2]

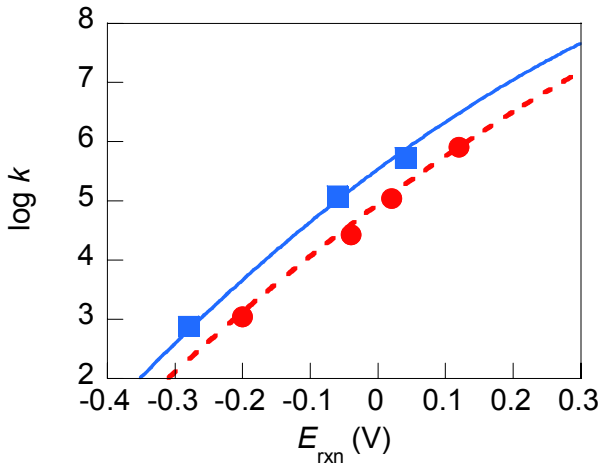

Figure S13. Relation between k and E_{rxn} (V) for the reactions **HOAr-CH$_2$py** + $[NAr_3]^{+\bullet}$ (■, solid line). Rates for **HOAr-C(Ph)$_2$NH$_2$** + $[NAr_3]^{+\bullet}$ (●, dashed line) from reference 2 are included for comparison. The curves are the fit to $k = Z\, e^{-[(\lambda - E_{rxn})^2/4\lambda k_B T]}$ with log(Z/M^{-1}s^{-1}) = 9.5 and 10.4.

B. Temperature dependence and isotope effect experiments

The temperature dependence kinetics for **HOAr-CH_2py** + $[Fe(Me_2bpy)_3]^{3+}$ were performed under pseudo-first order conditions with a 6-50-fold excess of phenol at various temperatures. The slope of k_{obs} vs. **[HOAr-CH_2py]** was taken as the second-order rate constant. The rate constants are listed in Table S10 and plotted in Figure S14a. A summary of the rate constants vs. temperature is on Table S11 and Figure S15.

The isotope effect kinetics for **DOAr-CH_2py** + $[Fe(5,5'\text{-}Me_2bpy)_3](PF_6)_3$ were performed with a 10-50-fold excess of phenol in MeCN with 1% CD_3OD, and fit to pseudo-first order kinetics. The slope is taken as the second-order rate constant. Control experiments were performed for this reaction under the same conditions except benchtop CH_3OH (1%) was used in place of d_4-methanol; the rates of these reactions were found to be within error of those performed without methanol. The rate constants are listed in Tables S10 and S12 and plotted in Figure S14b. A summary of the rate constants vs. temperature is in Tables S11 and S13.

(a) b)

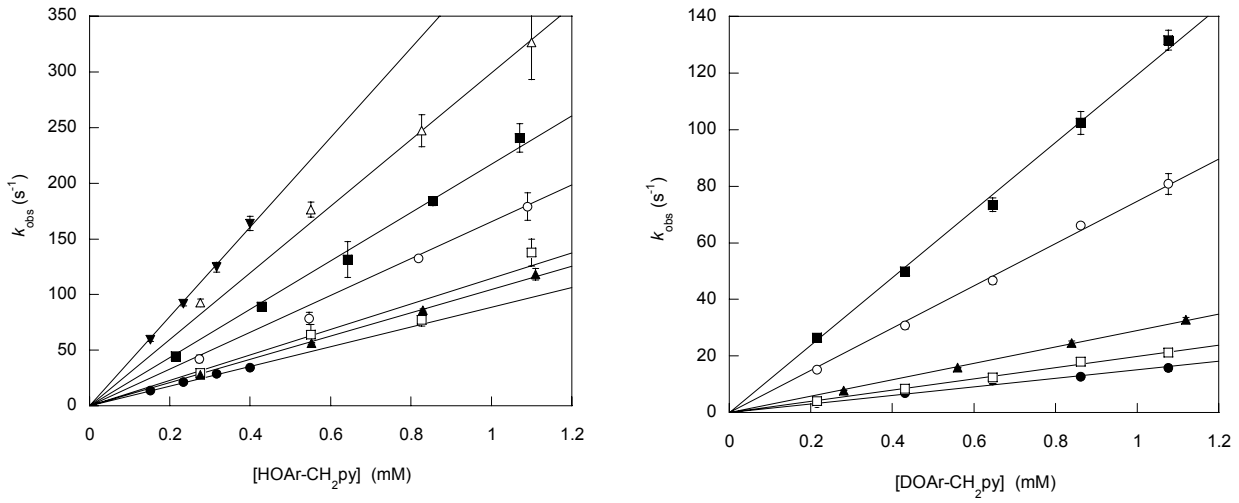

Figure S14. Pseudo-first order rate constants vs. phenol concentration for: [a] **HOAr-CH_2py** + $[Fe(Me_2bpy)_3]^{3+}$. Temperatures in K: 278.2 (●), 282.7 (□), 286.2 (▲), 297 (○), 308.2 (■), 319.7 (△), and 328.7 (▼). [b] **DOAr-CH_2py** + $[Fe(Me_2bpy)_3]^{3+}$. Temperatures in K: 279 (●), 287 (□), 297 (▲), 319 (○), and 328 (■).

Table S10. Pseudo-first order rate constants vs. phenol concentration for **HOAr-CH$_2$py** + $[Fe(Me_2bpy)_3]^{3+}$.

T (°C)	[phenol] (mM)	k_{obs} (s^{-1})	σ	T (°C)	[phenol] (mM)	k_{obs} (s^{-1})	σ
5.0	0.15	13.8	0.44	24.0 [a]	0.28	38.1	0.16
	0.23	21.3	0.67		0.56	79.7	0.9
	0.32	29	2.0		0.84	125	2
	0.40	34	1.2		1.12	163	4
6.0 [a]	0.22	21.2	0.9	35.0	0.21	44	1.9
	0.43	42.4	1.7		0.43	89.3	0.96
	0.65	73	5		0.64	130	16
	0.86	122	2		0.86	184	4.1
	1.1	99	9		1.1	240	13
9.5	0.28	29	2.6	46.5	0.28	93	3.4
	0.55	64	8.9		0.55	176	6.7
	0.83	77	5.4		0.83	250	15
	1.1	140	12		1.1	330	33
	1.4	160	12		1.4	409	11
13.0	0.28	27.7	0.77	47.0 [a]	0.215	64.8	1.2
	0.55	56.3	0.68		0.431	131	7
	0.83	86	1.19		0.646	190	22
	1.1	118	5.16		0.862	260	20
	1.4	144	1.49				
24.0	0.27	42	3.4	55.5	0.151	60	1.7
	0.55	79	5.5		0.234	92	2.0
	0.82	132.5	0.88		0.316	124	4.3
	1.1	180	12		0.399	164	6.3
	1.4	240	30				

[a] These experiments were performed in the presence of 1 % CH_3OH.

Table S11. Summary of temperature dependence data for **HOAr-CH$_2$py** + $[Fe(Me_2bpy)_3]^{3+}$.

T (K)	k (M^{-1} s^{-1})	T (K)	k (M^{-1} s^{-1})
278.2	$(9.2 \pm 0.9) \times 10^4$	297.2[a]	$(1.50 \pm 0.15) \times 10^5$
279.2[a]	$(1.0 \pm 0.2) \times 10^5$	308.2	$(2.5 \pm 0.3) \times 10^5$
282.7	$(1.12 \pm 0.11) \times 10^5$	319.7	$(3.0 \pm 0.3) \times 10^5$
286.2	$(1.05 \pm 0.11) \times 10^5$	320.2[a]	$(3.1 \pm 0.3) \times 10^5$
297.2	$(1.66 \pm 0.16) \times 10^5$	328.7	$(4.1 \pm 0.5) \times 10^5$

[a] These experiments were performed in the presence of 1 % CH_3OH.

Table S12. Pseudo-first order rate constants vs. phenol concentration for **DOAr-CH$_2$py** + $[Fe(Me_2bpy)_3]^{3+}$.

T (°C)	[phenol] (mM)	k_{obs} (s^{-1})	σ	T (°C)	[phenol] (mM)	k_{obs} (s^{-1})	σ
6	0.215	3.4	0.5	46	0.215	15.16	0.80
	0.431	6.8	0.3		0.431	30.74	1.23
	0.646	11.4	1.5		0.646	46.62	1.20
	0.862	12.6	0.7		0.862	66.15	0.81
	1.077	15.7	1.1		1.077	80.82	3.68
14	0.215	3.98	0.06	55	0.215	26.5	0.9
	0.431	8.35	0.13		0.431	49.9	0.8
	0.646	12.46	0.49		0.646	73.4	2.4
	0.862	17.95	0.21		0.862	102.4	4.1
	1.077	21.20	1.29		1.077	131.6	3.5
24	0.280	7.80	0.07				
	0.560	15.88	0.09				
	0.839	24.58	0.79				
	1.119	32.75	0.79				
	1.399	40.57	0.88				

Table S13. Summary of temperature dependence data for **DOAr-CH$_2$py** + $[Fe(Me_2bpy)_3]^{3+}$.

T (K)	k (M^{-1} s^{-1})	T (K)	k (M^{-1} s^{-1})
279	$(1.45 \pm 0.15) \times 10^4$	319	$(7.5 \pm 0.8) \times 10^4$
287	$(2.0 \pm 0.2) \times 10^4$	328	$(1.20 \pm 0.12) \times 10^5$
297	$(2.9 \pm 0.3) \times 10^4$		

VII. Calculations

Calculations were performed using Gaussian03.[8] In all cases, methyl groups were used in place of *tert*-butyls. The two phenyl groups in **HOAr-C(Ph)$_2$NH$_2$** were replaced with hydrogens, **HOAr-CH$_2$NH$_2$**. All optimized geometries were confirmed to be local minima by vibrational analysis. Energies are not corrected for zero-point vibrational energy. When indicated a polarized continuum model (PCM) of acetonitrile solvent was used as implemented in Gaussian. All geometries were optimized at the (U)B3LYP/6-31G* level. It was shown for **HOAr-py** and **$^{\bullet}$OAr-pyH^{+}** that optimization using larger basis sets (up to 6-311+G**) or with the inclusion of a solvent model produced geometries which were energetically equivalent (at (U)B3LYP/cc-pVTZ, with or without solvent model) to those produced with 6-31G*, Table S14.

A schematic representation of the four points of the energetic cycle used to calculate λ is shown in Figure S15. Qualitatively similar results for these calculations to those reported in Table 3 of the text were obtained at the B3LYP/6-31G*, B3LYP/6-311+G**, HF/6-311+G**, and MP2/6-311+G** levels of theory without a solvent model, Table S15. In all three phenol-base systems studied, geometries corresponding to the non-proton transferred phenol radical cation ([**HOAr-B**]$^{\bullet+}$) or the zwitterions ($^{-}$**OAr-BH**$^{+}$) could not be located as local minima at the B3LYP/6-31G* level of theory.

Heavy-atom bond lengths are given in Tables S16-S18. Cartesian coordinates for the optimized geometries of the neutral and radical cation species are given in Tables S19-S24.

(8) Gaussian 03, Revision D.02, M. J. Frisch, G. W. Trucks, H. B. Schlegel, G. E. Scuseria, M. A. Robb, J. R. Cheeseman, J. A. Montgomery, Jr., T. Vreven, K. N. Kudin, J. C. Burant, J. M. Millam, S. S. Iyengar, J. Tomasi, V. Barone, B. Mennucci, M. Cossi, G. Scalmani, N. Rega, G. A. Petersson, H. Nakatsuji, M. Hada, M. Ehara, K. Toyota, R. Fukuda, J. Hasegawa, M. Ishida, T. Nakajima, Y. Honda, O. Kitao, H. Nakai, M. Klene, X. Li, J. E. Knox, H. P. Hratchian, J. B. Cross, V. Bakken, C. Adamo, J. Jaramillo, R. Gomperts, R. E. Stratmann, O. Yazyev, A. J. Austin, R. Cammi, C. Pomelli, J. W. Ochterski, P. Y. Ayala, K. Morokuma, G. A. Voth, P. Salvador, J. J. Dannenberg, V. G. Zakrzewski, S. Dapprich, A. D. Daniels, M. C. Strain, O. Farkas, D. K. Malick, A. D. Rabuck, K. Raghavachari, J. B. Foresman, J. V. Ortiz, Q. Cui, A. G. Baboul, S. Clifford, J. Cioslowski, B. B. Stefanov, G. Liu, A. Liashenko, P. Piskorz, I. Komaromi, R. L. Martin, D. J. Fox, T. Keith, M. A. Al-Laham, C. Y. Peng, A. Nanayakkara, M. Challacombe, P. M. W. Gill, B. Johnson, W. Chen, M. W. Wong, C. Gonzalez, and J. A. Pople, Gaussian, Inc., Wallingford CT, 2004.

Table S14. B3LYP/cc-pVTZ absolute and relative energies for **HOAr-py** and **$^{\bullet}$OAr-pyH^{+}** at geometries optimized with various basis sets.[a]

Energy:	(U)B3LYP/cc-pVTZ//		(U)B3LYP/cc-pVTZ with solvent (MeCN) modeled using PCM		
Geometry:	B3LYP/6-31G*	B3LYP/6-311+G**	B3LYP/6-31G*	B3LYP/6-31G* w/ solvent model	B3LYP/ 6-311+G**
HOAr-py	-633.43441	-633.43488	-633.44431	-633.44429	-633.44465
	0.0	*-0.3*	*-6.2*	*-6.2*	*-6.4*
$^{\bullet}$OAr-pyH^{+}	-633.18307	-633.18355	-633.25586	-633.25608	-633.2562
	0.0	*-0.3*	*-45.7*	*-45.8*	*-45.9*

[a] Absolute energies are in hartrees, energies relative to (U)B3LYP/cc-pVTZ//B3LYP/6-31G* are in italics and are in kcal mol^{-1}.

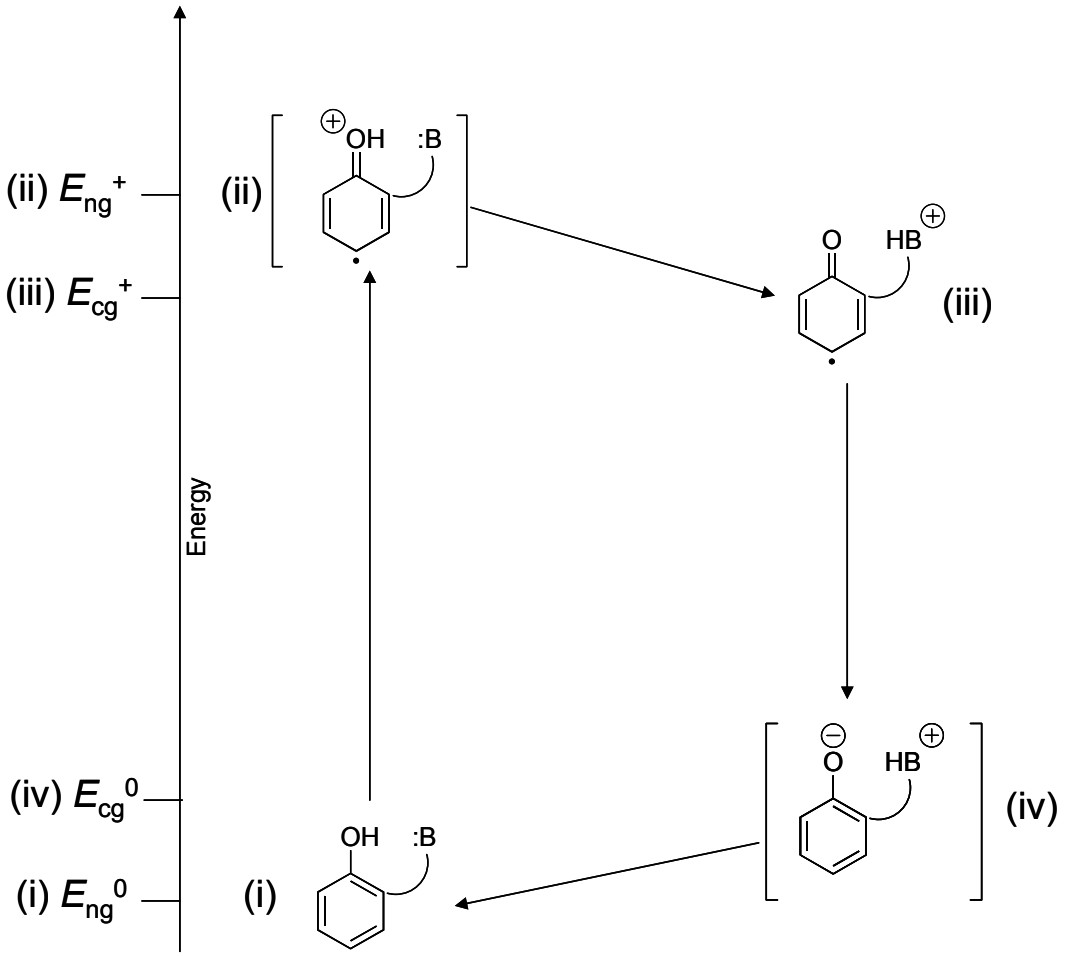

Figure S15. Schematic representation of the energetic cycle used to calculate inner-sphere reorganization energies for the theoretical CPET self-exchange reactions, **HOAr-B** + **$^{\bullet}$OAr-BH^{+}** = **$^{\bullet}$OAr-BH^{+}** + **HOAr-B**, $\lambda_{se,in} = (E_{ng}^{+} - E_{cg}^{+}) + (E_{cg}^{0} - E_{ng}^{0})$.

Table S15. Calculated gas phase inner-sphere reorganization energies ($\lambda_{se,in}$) at different levels of theory.[a]

-B	(U)B3LYP/ 6-31G*	(U)B3LYP/ 6-311+G**	(RO)HF/ 6-311+G**	(RO)MP2/ 6-311+G**
-py	24.7	23.8	30.2	29.3
-CH_2NH_2	35.6	34.1	38.3	38.9
-CH_2py	41.9	40.0	45.5	46.0

[a] Energies are reported in kcal mol^{-1} using single energy calculations at the level reported on (U)B3LYP/6-31G* geometries.

Table S16. Calculated heavy-atom bond lengths and their change upon oxidation for **HOAr-py**.[a]

Bond	HOArB	$^{\bullet}$OArBH$^+$	Δ^b
C1-O	1.348	1.258	-0.090
C1-C2	1.421	1.475	0.054
C2-C3	1.413	1.386	-0.027
C3-C4	1.387	1.414	0.027
C4-C5	1.407	1.415	0.008
C5-C6	1.387	1.378	-0.009
C6-C1	1.415	1.466	0.051
C2′-C3′	1.412	1.404	-0.008
C3′-C4′	1.387	1.390	0.003
C4′-C5′	1.397	1.401	0.004
C5′-C6′	1.389	1.381	-0.008
C6′-N	1.337	1.347	0.010
N-C2′	1.356	1.363	0.007
C2-C2′	1.479	1.469	-0.010
C4-CH_3	1.511	1.500	-0.011
C6-CH_3	1.507	1.497	-0.010
		RMS:	0.032[c]

[a]All distances are in Å, calculated at B3LYP/6-31G*. [b] Difference in bond length between neutral and radical cation. [c] Root mean square of Δ for the bond lengths reported here.

Table S17. Calculated heavy-atom bond lengths and their change upon oxidation for **HOAr-CH_2py**. [a]

Bond	HOArB	$^{\bullet}$OArBH$^+$	Δ^b
C1-O	1.364	1.268	-0.096
C1-C2	1.407	1.460	0.053
C2-C3	1.400	1.373	-0.027
C3-C4	1.395	1.425	0.030
C4-C5	1.402	1.409	0.007
C5-C6	1.394	1.383	-0.011
C6-C1	1.409	1.450	0.041
C2′-C3′	1.399	1.393	-0.006
C3′-C4′	1.393	1.396	0.003
C4′-C5′	1.395	1.399	0.004
C5′-C6′	1.393	1.384	-0.009
C6′-N	1.338	1.347	0.009
N-C2′	1.346	1.354	0.008
C2-CH_2	1.523	1.523	0.000
CH_2-C2′	1.517	1.516	-0.001
C4-CH_3	1.517	1.501	-0.016
C6-CH_3	1.508	1.498	-0.010
		RMS:	0.031[c]

[a]All distances are in Å, calculated at B3LYP/6-31G*. [b] Difference in bond length between neutral and radical cation. [c] Root mean square of Δ for the bond lengths reported here.

Table S18. Calculated heavy-atom bond lengths and their change upon oxidation for **HOAr-CH_2NH_2**.[a]

Bond	HOArB	$^{\bullet}$OArBH$^+$	Δ[b]
C1-O	1.362	1.27	-0.092
C1-C2	1.408	1.461	0.053
C2-C3	1.400	1.371	-0.029
C3-C4	1.395	1.427	0.032
C4-C5	1.403	1.409	0.006
C5-C6	1.394	1.385	-0.009
C6-C1	1.408	1.457	0.049
N-CH_2	1.481	1.519	0.038
C2-CH_2	1.513	1.508	-0.005
C4-CH_3	1.512	1.500	-0.012
C6-CH_3	1.507	1.497	-0.010
		RMS:	0.040[c]

[a]All distances are in Å, calculated at B3LYP/6-31G*. [b] Difference in bond length between neutral and radical cation. [c] Root mean square of Δ for the bond lengths reported here.

Table S19. Cartesian coordinates for optimized geometry of **HOAr-py**.

atom	x	y	z
C1	2.918605	0.189568	-0.000069
C2	2.236126	1.419993	0.000039
C3	0.849790	1.389959	0.000085
C4	0.109467	0.186315	0.000044
C5	0.837204	-1.034134	-0.000009
C6	2.252369	-1.026975	-0.000088
C7	-1.369677	0.204767	0.000027
C8	-2.131143	1.393400	-0.000211
C9	-3.516995	1.327635	-0.000217
C10	-4.151448	0.082493	-0.000013
C11	-3.342706	-1.046984	0.000156
N12	-2.006876	-0.991980	0.000198
C13	2.999068	2.724526	0.000150
C14	2.986447	-2.343188	-0.000179
O15	0.252169	-2.248158	0.000079
H16	4.007594	0.187272	-0.000165
H17	0.323590	2.339125	0.000219
H18	-1.646309	2.361393	-0.000421
H19	-4.101339	2.244013	-0.000392
H20	-5.232609	-0.008827	-0.000006
H21	-3.774567	-2.045618	0.000327
H22	3.646519	2.814849	-0.881611
H23	3.646360	2.814788	0.882030
H24	4.069665	-2.186783	-0.000362
H25	2.721819	-2.945508	-0.877354
H26	2.722144	-2.945447	0.877155
H27	-0.734685	-2.087937	0.000146
H28	2.319943	3.583557	0.000131

Table S20. Cartesian coordinates for optimized geometry of **$^{\bullet}$OAr-pyH^{+}**.

atom	x	y	z
C1	2.957393	0.168247	-0.001385
C2	2.261015	1.399824	-0.001365
C3	0.847197	1.391839	-0.001237
C4	0.110898	0.217424	-0.000310
C5	0.837640	-1.066309	0.000231
C6	2.303697	-1.044545	-0.000499
C7	-1.357937	0.245167	-0.000290
C8	-2.154029	1.402218	-0.001255
C9	-3.540080	1.299398	-0.000959
C10	-4.162058	0.043660	0.000297
C11	-3.357716	-1.079457	0.001179
N12	-2.017525	-0.947953	0.000875
C13	3.020025	2.694085	0.002230
C14	3.019640	-2.358871	-0.000648
O15	0.240713	-2.174053	0.001038
H16	4.044418	0.185470	-0.002231
H17	0.347663	2.354850	-0.001898
H18	-1.691870	2.380425	-0.002260
H19	-4.142439	2.202544	-0.001714
H20	-5.240766	-0.058267	0.000559
H21	-3.738510	-2.094264	0.002136
H22	2.357889	3.562360	-0.038796
H23	3.707481	2.743523	-0.851467
H24	4.102843	-2.218771	-0.000545
H25	2.738068	-2.954503	-0.876881
H26	2.737847	-2.954868	0.875239
H27	-1.377384	-1.773321	0.001393
H28	3.637617	2.776835	0.906101

Table S21. Cartesian coordinates for optimized geometry of **HOAr-CH_2NH_2**.

atom	x	y	z
C1	0.007327	0.013375	0.000777
C2	0.015406	-0.007860	1.403342
C3	1.255611	0.001976	2.042711
C4	2.457591	0.036434	1.326236
C5	2.413910	0.037403	-0.080751
C6	1.177930	0.030811	-0.756414
C7	-1.276841	-0.045337	2.186949
C8	1.157480	0.040677	-2.263871
O9	3.547807	0.056039	-0.835259
H10	-0.947466	0.005746	-0.523336
H11	1.296001	-0.007509	3.131206
H12	-1.849276	-0.960201	1.984587
H13	-1.928649	0.800760	1.934469
H14	0.131535	-0.003246	-2.642796
H15	1.716801	-0.809009	-2.673164
H16	1.633970	0.943804	-2.664352
H17	4.288839	-0.225863	-0.237053
H18	-1.089244	-0.006904	3.265225
C19	3.784913	0.139064	2.045821
N20	4.796213	-0.750680	1.429928
H21	3.640176	-0.050545	3.120043
H22	4.182235	1.159946	1.954741
H23	4.544596	-1.725963	1.585480
H24	5.711362	-0.602039	1.850834

Table S22. Cartesian coordinates for optimized geometry of **$^{\bullet}$OAr-$CH_2NH_3^+$**.

atom	x	y	z
O1	0.090140	-0.063510	0.076416
C2	0.023403	-0.011530	1.343305
C3	1.237736	-0.052841	2.153505
C4	1.149600	-0.064064	3.521933
C5	-0.114688	-0.012604	4.181374
C6	-1.287710	0.055417	3.403536
C7	-1.266093	0.060556	2.018706
C8	2.568493	0.032097	1.448894
N9	2.553423	-0.838426	0.204711
C10	-2.505242	0.116943	1.181140
C11	-0.171374	-0.021908	5.680081
H12	1.604211	-0.607839	-0.236710
H13	3.327425	-0.630585	-0.433349
H14	2.577554	-1.837696	0.431424
H15	2.052234	-0.093169	4.129013
H16	-2.245883	0.100064	3.914225
H17	3.402975	-0.269683	2.084607
H18	2.756455	1.047552	1.083632
H19	-3.400226	0.198708	1.801804
H20	-2.469937	0.968824	0.492168
H21	-2.591464	-0.778298	0.553578
H22	0.320983	-0.915450	6.085384
H23	-1.199252	0.000388	6.048423
H24	0.360581	0.844341	6.095386

Table S23. Cartesian coordinates for optimized geometry of **HOAr-CH$_2$py**.

atom	x	y	z
C1	1.041550	0.931426	0.372601
C2	0.619131	-0.377324	0.669407
C3	1.459509	-1.449154	0.344047
C4	2.710667	-1.258715	-0.243818
C5	3.116219	0.059318	-0.494607
C6	2.309976	1.157680	-0.198034
C7	-0.696095	-0.628597	1.395343
C8	-1.935108	-0.407291	0.549162
N9	-2.207011	0.870381	0.223892
C10	-3.282087	1.137102	-0.526730
C11	-4.151265	0.151042	-0.988352
C12	-3.875286	-1.174723	-0.654970
C13	-2.754051	-1.458237	0.121998
C14	2.754715	2.571110	-0.477042
C15	3.597185	-2.428788	-0.604623
O16	0.284889	2.030318	0.657304
H17	-0.674368	1.790359	0.610201
H18	4.092997	0.238205	-0.941844
H19	1.129254	-2.460675	0.576389
H20	-0.761728	0.039965	2.264961
H21	-0.700551	-1.654001	1.778077
H22	-3.450065	2.185509	-0.763595
H23	-5.013635	0.417426	-1.591117
H24	-4.524729	-1.977076	-0.994817
H25	-2.511510	-2.479915	0.398264
H26	4.635772	-2.258931	-0.296178
H27	3.254353	-3.351815	-0.124705
H28	3.610734	-2.609734	-1.688152
H29	2.039195	3.090263	-1.125376
H30	2.816816	3.160529	0.445825
H31	3.737073	2.585591	-0.959902

Table S24. Cartesian coordinates for optimized geometry of **$^{\bullet}$OAr-CH$_2$pyH$^+$**.

atom	x	y	z
C1	1.019072	0.902125	0.380309
C2	0.646909	-0.497510	0.568039
C3	1.540069	-1.482630	0.226841
C4	2.831541	-1.178487	-0.291603
C5	3.206954	0.171966	-0.438247
C6	2.357789	1.213294	-0.111137
C7	-0.674523	-0.834445	1.245463
C8	-1.936956	-0.520015	0.470749
N9	-2.161010	0.773838	0.142279
C10	-3.259909	1.204444	-0.507475
C11	-4.242931	0.300296	-0.870021
C12	-4.055650	-1.049192	-0.553751
C13	-2.902155	-1.459480	0.116559
C14	2.740856	2.653675	-0.261499
C15	3.774797	-2.291905	-0.641562
O16	0.203796	1.841734	0.624994
H17	-1.369580	1.425773	0.392805
H18	4.198132	0.398362	-0.822433
H19	1.275227	-2.527910	0.371777
H20	-0.728193	-0.289035	2.198660
H21	-0.689536	-1.898894	1.491739
H22	-3.311328	2.267061	-0.715117
H23	-5.129901	0.644088	-1.389247
H24	-4.809255	-1.780973	-0.828370
H25	-2.749475	-2.502166	0.371805
H26	4.063125	-2.852349	0.258260
H27	3.301929	-3.011553	-1.321350
H28	4.687110	-1.919324	-1.113082
H29	2.061997	3.168478	-0.951499
H30	2.657876	3.179854	0.696630
H31	3.763401	2.755050	-0.632470